On the origin of anomalous birefringence in grandite garnets

Article *in* Mineralogical Magazine · June 2001

DOI: 10.1180/002646101300119538

CITATIONS
42

READS
200

5 authors, including:

O. V. Frank-Kamenetskaya
Saint Petersburg State University
98 PUBLICATIONS **846** CITATIONS

SEE PROFILE

Mineralogical Magazine, June 2001, Vol. 65(3), pp. 445–459

On the origin of anomalous birefringence in grandite garnets

A. G. SHTUKENBERG*, YU. O. PUNIN, O. V. FRANK-KAMENETSKAYA, O. G. KOVALEV AND P. B. SOKOLOV

Department of Crystallography, Saint-Petersburg State University, Universitetskaya nab., 7/9, 199034, Saint Petersburg, Russia

ABSTRACT

The origin of anomalous birefringence of grossular–andradite (grandite) garnets from skarns in Mali and Russia was considered. The crystals had complex optical patterns which can be induced by superposition of two phenomena: mismatch compositional strain (stress birefringence) and growth ordering of atoms (growth dissymmetrization). Study of the crystals using several experimental techniques (optical microscopy, microprobe analysis, X-ray diffraction topography and X-ray single crystal diffraction) as well as calculations of anomalous birefringence has confirmed this hypothesis. Depending on the crystal composition and growth conditions, the relative magnitude of each phenomenon controls the various optical effects. As a result one can see two groups of crystals which are found to have fundamentally different anomalous optical properties: crystals with low (<0.001) and high (0.001−0.015) values of birefringence. The spatial distribution of birefringence within each group is different and this fact is related to different mechanisms causing optical anomalies: stress birefringence and growth dissymmetrization for these two groups, respectively.

KEYWORDS: birefringence, stress birefringence, growth dissymmetrization, grandite garnet, Mali, Russia.

Introduction

GARNETS of the grossular–andradite series $X_3Y_2(SiO_4)_3$, $X = Ca^{2+}$, $Y = Al^{3+}$, Fe^{3+} (grandite garnets) belong to the cubic system (space group $Ia\bar{3}d$) and therefore should be optically isotropic. It is known that the end-members of the series are usually isotropic, whereas intermediate members often reveal anomalous birefringence (McAloon and Hofmeister, 1995). The origin of this birefringence remains unclear in spite of a significant number of papers devoted to the study of this phenomenon, e.g. Brauns (1891), Akizuki (1984), McAloon and Hofmeister (1995, and references therein). The complexity of this problem is caused, in particular, by widely variable optical patterns. Grandite garnet crystals reveal significant optical inhomogeneities, namely, concentric zoning, sector zoning, subsector zoning, block structures and wavy and spotty extinction. Isotropic and anisotropic crystals may be found together in the same occurence or even within a single sample.

In order to explain the origin of optical anomalies in grandites various causes were considered: (1) lowering of the cubic symmetry due to the long-range ordering of atoms and their groups including: (a) partial ordering of Al^{3+} and Fe^{3+} on octahedral sites Y (Akizuki, 1984); (b) partial ordering of Ca^{2+} and impurities of Fe^{2+}, Mg^{2+} and Mn^{2+} on dodecahedral X sites (Griffen *et al.*, 1992); (c) orientation ordering of OH^- groups replacing Si in tetrahedral sites (Rossman and Aines, 1986); and (d) ordering of rare-earth elements on octahedral Y sites resulting in a magneto-optic effect (Blanc and Maisonneuve, 1973); and (2) mismatch-strain related to compositional inhomogeneity (Lessing and Standish, 1973; McAloon and Hofmeister, 1995).

In this paper we consider only grandite garnets ($Ca_3(Al,Fe)_2(SiO_4)_3$) with small amounts of impurities. Therefore, mechanisms 1b, c and d are unlikely to contribute significantly to the formation of optical anomalies in such crystals and so these mechanisms will not be considered.

* E-mail: sasha@as3607.spb.edu

Thus, there are only two mechanisms (1a and 2) to account for optical anomalies in most grandite garnets. However, we should not exclude the influence of other mechanisms in special cases.

Mechanism 1a has been suggested for grandite garnets many times and there are a lot of experimental data which support this hypothesis (Akizuki, 1984; Akizuki *et al.*, 1998; Allen and Buseck, 1988; Takéuchi *et al.*, 1982). On the other hand, although mechanism 2 has been mentioned in some papers, no systematic studies of grandite garnets are available. This was the first aim of our study, namely, to understand the contribution of mismatch strain (mechanism 2) to the origin of anomalous birefringence in grandite garnets. If both mechanisms (1a and 2) operate in garnets, the following questions are to be answered: how do we distinguish the two mechanisms using the observed optical properties, and what growth conditions favour one mechanism over the other? An attempt to answer these questions is the second aim of the paper.

We carried out an experimental study of twenty grandite crystals (#1–20) from limestone skarns of Mali (West Africa) and three crystals (#21–23) from skarns of Dalnegorsk (Russia). These garnets are big, transparent crystals with various compositions, colours, imperfections and optical anomalies and therefore were very suitable for our investigation. A number of experimental techniques was applied: optical microscopy was used to measure the optical properties, X-ray single crystal diffraction methods were applied to test the crystal symmetry, microprobe analysis and infra-red (IR) spectroscopy provided data on overall and local chemical composition, microprobe analysis, powder X-ray diffraction (XRD) and XRD topography studies were performed to reveal and estimate mismatch strain.

Experimental

The crystals studied were 0.5–7 cm in diameter and they exhibited dodecahedral habits. Plates normal to [001], [110] or [111] were cut from the crystals and studied with a polarizing microscope and by microprobe analysis. Birefringence was measured with a Berek compensator with an accuracy of 10–20%, depending on the value of birefringence and the thickness of the sample. Electron microprobe analysis was performed (using Camebax and Camscan microanalysers) by Yu.L. Krezer and L.S. Smolskaya.

Some of the samples with different birefringence were studied in detail using the following experimental techniques. Transmission IR spectra on powder samples (#1 (core), #2, #3, #4 and #5) were collected by M.L. Zorina in the energy range 3400–3800 cm^{-1} using an IR spectrometer with a resolution of 2.0 cm^{-1}. Samples for this study were prepared in a form of vaseline suspension placed between two KBr plates. X-ray diffraction topographs (samples #5 and #21) were recorded by A.E. Voloshin using the Lang technique (Mo-$K\alpha$ radiation). Average cubic lattice constants (samples #1 (core), #2 (rim), #3, #4 and #5) were measured by the X-ray powder diffraction method (diffractometer DRON-2.0, Co-$K\alpha$ radiation, internal standard Si). Analysis of the crystal symmetry (samples #1 (core), #1 (rim) and #3) was performed for spherical samples (0.155 ± 0.005 mm in radius) in a Syntex $P2_1$ four-circle autodiffractometer (Mo-$K\alpha$ radiation, graphite monochromator). The intensities of the reflections were measured using the ω-method. Single crystal lattice constants were calculated by the least-squares method using 24 reflections (2 2 12, 648, 12 0 0 and their equivalents in the Laue class $m\bar{3}m$).

Samples

The composition of the crystals studied is described by the following formula: $(Ca_{2.9-3.0}Mn_{0.00-0.02}Mg_{0.00-0.06})^{VIII}(Al_{0.0-2.0}Fe_{0.0-2.0}Ti_{0.0-0.11})^{VI}(SiO_4)_3$. One can see that the level of impurities in X sites is insignificant. According to the IR spectroscopy data these samples contain no water (<0.01%), since no absorption bands are observed in the OH-stretching region. Thus, the composition of these crystals is close to $Ca_3(Al,Fe)_2(SiO_4)_3$. Microprobe data obtained for some samples (Table 1) show considerable compositional inhomogeneity of the crystals studied. The degree of inhomogeneity differs among the crystals, from relatively homogeneous (e.g. #3) to very inhomogeneous (e.g. #20). As expected from stoichiometric relations, Al_2O_3 and Fe_2O_3 show a distinct antipathetic relation.

The crystals studied have various colours and display colour zonation. The colour reflects the chemical composition. Colourless and green parts of the crystals typically contain a small amount of Ti (up to 0.25 at.%) and Mn (up to 0.1 at.%). In this case green parts correspond to a higher concentration of Fe. Brown parts of the crystals

TABLE 1. Variations of the chemical composition (wt.%) in the crystals studied.

Samples	1	2	3	4	5	8	11	16	17	19	20	21
SiO_2	36.67–39.35	36.57–40.21	37.74–39.47	37.13–38.79	37.91–39.06	37.94–39.36	36.93–38.06	36.39–39.45	35.28–38.83	37.07–38.93	35.03–38.48	33.46–38.79
TiO_2	0.00–0.89	0.00–1.04	0.02–0.72	0.97–2.14	0.00–0.51	0.15–0.64	0.94–2.00	0.07–1.56	0.45–2.19	0.01–1.69	0.01–2.29	0.00–0.51
Al_2O_3	10.26–18.77	11.11–19.07	15.74–17.82	10.26–13.17	9.76–16.71	13.24–18.03	10.50–12.88	10.46–16.76	11.24–19.31	9.12–16.34	5.98–17.53	0.45–13.52
Fe_2O_3	7.21–15.93	4.37–15.11	7.04–9.33	12.95–16.53	7.49–18.04	5.60–12.75	12.70–16.07	7.50–16.45	11.35–16.24	7.30–18.36	6.63–21.72	13.70–32.03
MgO	0.00	0.00	0.00	0.00	0.51–0.94	0.28–0.68	0.30–0.62	0.00–0.90	0.03–1.00	0.18–0.81	0.00–1.24	0.00–0.49
CaO	35.35–38.96	36.67–39.78	35.19–37.41	35.15–36.38	33.72–34. 91	34.45–36.20	34.08–34.64	33.10–34.98	34.80–37.89	34.15–35.92	35.03–38.48	31.83–35.51
MnO	0.00–0.55	0.00–0.25	0.68–1.22	0.16–0.55	0.00–0.60	0.04–0.63	0.18–0.48	0.00–0.63	0.00–0.26	0.00–0.26	0.05–0.24	0.05–0.55
Fe/(Fe+Al)	0.22–0.50	0.13–0.42	0.22–0.28	0.38–0.51	0.23–0.54	0.17–0.38	0.39–0.50	0.17–0.49	0.17–0.47	0.22–0.56	0.19–0.72	0.55–0.98

may contain the same concentration of Fe as green ones. However, the Ti and Mn contents may be considerably greater (up to 1.1 and 0.2 at.%, respectively).

The optical patterns observed are diverse. However, they may be divided into two groups with fundamentally different optical properties. The main difference between these groups is the value of birefringence. The crystals and parts of crystals having low (<0.001) and high (0.001−0.015) birefringence, belong to the first and the second groups, respectively (Table 2). It is important to note that any crystal can be formed by zones belonging to either or both groups.

Group 1 is characterized by distinct fine optical zoning visible in polarized light (thicknesses from several μm up to 0.5 mm). Within each zone both the birefringence and orientation of the optical indicatrix are usually constant, although significant distinctions of birefringence and extinction position (either 5−15° or ~90° relative to the boundaries of the zones) can occur in neighbouring zones. Numerous radial bands running from the crystal centre or from the boundaries of some zones superimpose on the zoning, resulting in a chess-board structure (Figs 1, 2). According to XRD topographic data, the positions of these optical bands correspond to those lines with strong contrast (dislocation bundles).

For Group 2 the distribution of the anomalous optical properties is more uniform. Here, a' is nearly normal to the growth front (110) in all cases (Fig. 3). Fine-scale zoning is rare. However, wedge-like bands nearly parallel (subparallel) to the growth front (subzones) are often visible. They adjoin the boundaries of the growth sectors or dislocation bundles and taper off towards the centre of the growth sectors. These subzones have similar birefringence but differ slightly (by a few degrees) in the extinction direction. In some crystals, cracks of a certain orientation (e.g. perpendicular to the growth direction) appear on these zone boundaries.

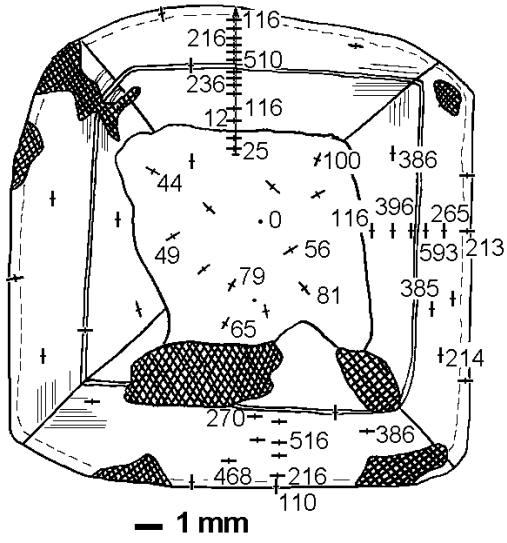

FIG. 1. Schematic diagram of the thin-section parallel to the (001) for crystal #2. Axial directions [110] and [$\bar{1}$10] are vertical and horizontal, respectively. Numbers refer to birefringence ($\times 10^{-6}$), crosses indicate orientation of extinction. Hatching corresponds to inclusions. Fine zoning is shown schematically by means of lines parallel to the four growth faces {110}. Microprobe analysis was carried out along the vertical line with the arrow.

Mismatch strain

Calculation of lattice constants

The crystals studied have a pronounced compositional inhomogeneity (especially zonal inhomogeneity) (Fig. 2) manifesting itself in changes of colour and refractive index, that can be seen using the Becké effect. The inhomogeneity should produce internal mismatch strain resulting in anomalous birefringence. This strain may be partly relaxed by plastic and brittle deformation that shows up in high dislocation densities

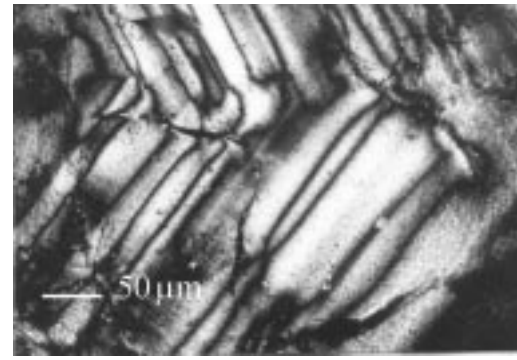

FIG. 2. Cross-polarizied photomicrograph of block-like structure with alternation of a' and c' orientation between the neighbouring zones. Boundaries between zones in two adjacent {211} growth sectors may be seen as narrow black lines. Crystal #1 (group 1), thin-section parallel to the (001) face.

TABLE 2. Characteristics of the garnets studied.

Group	Number of crystals with this group of optical patterns	Growth sectors	Thickness (mm)	Location in the crystal	Colour	Fine zoning in polarized light	Thickness of fine zones (μm)	Composition variations				Birefringence ($\times 10^{-4}$)
								Fe/(Fe+Al) (%)	Ti (at.%)	Mg (at.%)	Mn (at.%)	
1	13	{110}, {211} transforming into {110}	Up to 35	Central zones or the whole crystal	Colourless, light green, green, light brown	In most crystals; different orientation of indicatrix	3–20, up to 500	13–49	0–1.1	0–0.6	0–0.2	0–10, usually 0.6–6
2	18	{110} and small {211}	0.5–2.5 up to 8.5	Outer parts of crystal or the whole crystal	Various tints of brown, green, reddish-brown	Sometimes; different value of birefringence	3–60	22–55	0.2–0.6	0.2–0.55	0.03–0.4	9–145, usually >30

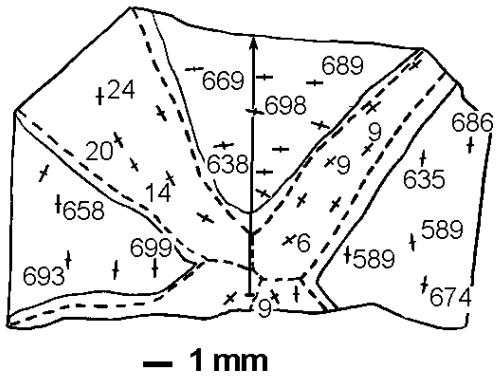

FIG. 3. Schematic diagram of the thin-section parallel to the (001) face for crystal #3. Numbers refer to the birefringence ($\times 10^{-5}$). Seven growth sectors of {110} are seen in this thin-section. For other designations, see Fig. 1.

(detected by XRD topography) and numerous cracks appearing at the zone boundaries. However, it is lilely that only a small part of the elastic strain relaxes.

To estimate quantitatively the contribution of strain to the optical anomalies, we have calculated the stress birefringence on the basis of the distribution of lattice constants in the crystal. This distribution is not easy to find by direct experiment. However, we can measure concentration profiles of elements using microprobe analysis and calculate the variation of lattice constants using numerous published empirical regression relations between the chemical composition of garnet (value Fe/(Al + Fe), average ionic radii for the X (R^{VIII}) and Y (R^{VI}) sites) and lattice constant a (Table 3). We have measured the lattice constants for several homogeneous parts of crystals with known chemical composition and showing sharp diffraction maxima, which allowed us to test and refine regression equations for our case (Table 3, Fig. 4). It was found that equation 8 provided the minimum difference between calculated and measured lattice constants (up to 0.006 Å) and, therefore, it was this equation that we used for our further calculations.

Although microprobe data contain errors, this fact does not influence significantly calculated values of mismatch strain and birefingence, since statistical errors are negligible ($\Delta a/a < 0.03\%$) and systematic errors change only the absolute values of concentrations and lattice constants. Calculating mismatch strains (see below) we took

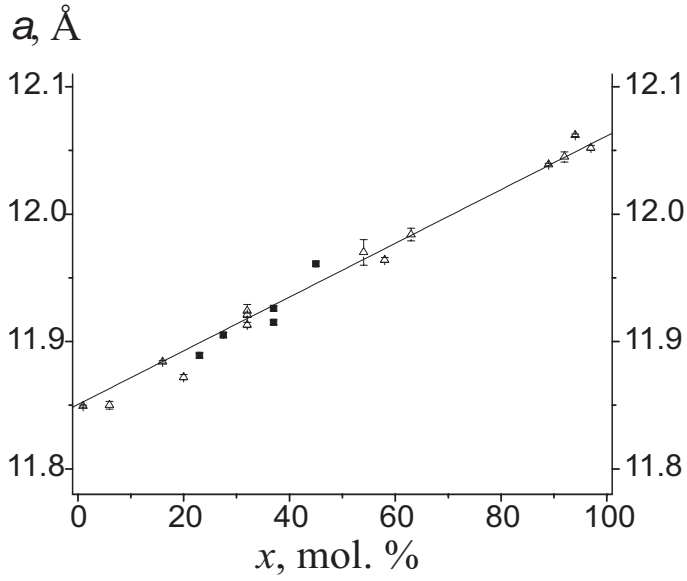

FIG. 4. Lattice constant (a) of grandite garnets as a function of their composition x = Fe/(Al + Fe). Squares – our data, triangles – literature data (Allen and Buseck, 1988; Hariya and Kimura, 1978; Murad, 1976; Takéuchi *et al.*, 1982).

TABLE 3. Chemical composition, calculated lattice constants (a) and measured lattice constant ($a_{powd.}$) of our grandite garnets.

Characteristics		Samples 1 (core)	1 (rim)	2 (core)	2 (rim)	3	4	5 (core)	5 (rim)
CaO (wt.%)		35.81	38.57	37.89	38.06	36.68	35.80	35.39	34.56
Al_2O_3 (wt.%)		13.65	16.02	18.64	12.96	17.10	11.70	14.63	15.74
Fe_2O_3 (wt.%)		12.36	7.21	4.48	12.16	7.84	14.94	10.87	9.49
SiO_2 (wt.%)		39.19	38.15	39.18	37.47	37.44	37.78	38.82	38.84
MnO (wt.%)		0.17	0.11	0.11	0.22	1.06	0.17	1.07	0.61
TiO_2 (wt.%)		0.13	0.75	0.23	0.45	0.15	0.17	0.52	0.52
Total		101.31	100.81	100.53	101.32	100.27	101.56	101.29	99.76
x = Fe/(Al+Fe)		0.37	0.22	0.13	0.37	0.23	0.45	0.32	0.28
R^{VIII} (Å)		1.1194	1.1173	1.1196	1.1193	1.1164	1.1194	1.1106	1.1178
R^{VI} (Å)		0.5704	0.5570	0.5450	0.5716	0.5551	0.5801	0.5685	0.5611
$a = 11.840 + 0.215 \times x$ (Å)	(I)	11.920	11.888	11.868	11.920	11.889	11.937	11.909	11.899
$a = 11.845 + 0.217 \times x$ (Å)	(II)	11.925	11.893	11.873	11.925	11.895	11.943	11.915	11.905
$a = 9.125 + 1.56R^{VIII} + 2.0R^{VI}$ (Å)	(III)	12.012	11.984	11.961	12.014	11.976	12.031	11.994	11.991
$a = 9.223 + 1.407R^{VIII} + 1.694R^{VI}$ (Å)	(IV)	11.764	11.740	11.721	11.766	11.734	11.781	11.749	11.746
$a = 9.9 + 1.212R^{VIII} + 1.464R^{VI}$ (Å)	(V)	12.091	12.071	12.054	12.093	12.065	12.106	12.078	12.076
$a = 9.336 + 2.1R^{VIII} + 1.286R^{VI}$ (Å)	(VI)	12.420	12.400	12.388	12.421	12.394	12.433	12.399	12.405
$a = 8.903 + 2.17R^{VIII} + 1.7R^{VI}$ (Å)	(VII)	12.301	12.276	12.258	12.303	12.269	12.318	12.279	12.282
$a = 9.04 + 1.61R^{VIII} + 1.89R^{VI}$ (Å)	(VIII)	**11.920**	**11.893**	**11.872**	**11.922**	**11.886**	**11.955**	**11.902**	**11.900**
$a_{powd.}$ (Å)		11.915(2)	–	–	11.926(2)	11.889(2)	11.961(2)	–	11.905(2)

Regression equations were taken from: I – McAloon and Hofmeister, 1995; II – Bird and Helgeson, 1980; III–VII – Vorobiev, 1989; VIII – Novak and Gibbs,1971 $R^{VIII} = \frac{\sum_i R_i^{VIII} m_i}{\sum_i m_i}$, $R^{VI} = \frac{\sum_k R_k^{VI} m_k}{\sum_k m_k}$ where R_i^{VIII} and R_k^{VI} are ionic radii according to Shannon (1976) for dodecahedral and octahedral sites; m_i and m_k are molar parts of cations occupying these sites, respectively

the differences between values of lattice constants in the neighbouring zones $\Delta a/a$, as systematic changes of lattice constants; they did not distort the results significantly.

Calculation of birefringence

Describing elastic strain in the thin-section cut from the crystal, we assumed that components of the stress tensor differ from zero value in the plane of the section only. This assumption is valid, because the diameter of the section is considerably greater than its thickness. The shape of any crystal in thin-section is close to circular (Fig. 1). This allows us to use the model of discrete concentric zoning (Gorskaya *et al.*, 1992). Following this model, a crystal can be described as consisting of N concentric zones j = 1,...N. The lattice constant and the outer radius of zone j are equal to a_j and r_j, respectively. The maximum shear stress in each zone is calculated as the mean value of the stresses on the inner and outer boundaries of the zone. In the isotropic approximation, it is equal (according to Gorskaya *et al.*, 1992) to:

$$(\tau_{max})_j = \frac{(\sigma_{rr})_j - (\sigma_{\theta\theta})_j}{2} = \frac{E}{4}\sum_{i=1}^{j}\frac{a_i - a_{i-1}}{a}\left(\frac{r_{i-1}^2}{r_j^2} + \frac{r_{i-1}^2}{r_{j-1}^2}\right)(a_0 = a_1) \quad (1)$$

where $(\sigma_{rr})_j$ and $(\sigma_{\theta\theta})_j$ are the main normal stresses in cylindrical coordinates and E is the Young modulus.

We analysed the thin-section which was cut parallel to the plane (001) of a garnet crystal, and a line in this section parallel to the [110] direction. This line coincided with the location of the microprobe profile measured for crystals #2 and #3 (Figs 1, 3). Along this line, stress birefringence in zone j (according to Nye, 1957) is equal to:

$$(\Delta n)_j = n^3\pi_{44}(\tau_{max})_j \quad (2)$$

where n is a refractive index and π_{44} the component of the piezo-optic tensor. Unfortunately, we were unable to find piezo-optic coefficient values corresponding to grandite garnets in the literature. Therefore, available experimental data for compounds with similar structure and chemical composition were used in order to estimate these quantities (Landolt and Börnstein, 1979). The value of π_{44} lies in the range $0.5-10\times10^{-12}$ Pa^{-1}. For synthetic rare-earth garnets this coefficient is $0.5-0.8\times10^{-12}$ Pa^{-1}. This value is the most likely for our crystals.

Analysis of results

Let us consider crystals with fundamentally different optical patterns, e.g. crystals #2 and #3, which according to their optical properties correspond to groups 1 and 2, respectively. The maximum value of the shear stress, τ_{max}, is equal to $2-3.5\times10^8$ Pa and 0.5×10^8 Pa in crystals #2 and #3, respectively (Figs 5, 6). The birefringence for crystal #2 is $<6\times10^{-4}$ and for crystal #3 is equal to $60-70\times10^{-4}$. Thus, the maximum values of shear stress and birefringence reveal an antipathetic relation. This fact is sufficient to show that the anomalous birefringence in these crystals has a different origin and strain is likely to be able to make a significant contribution to the optical anomalies only in crystal #2. However, this needs confirmation.

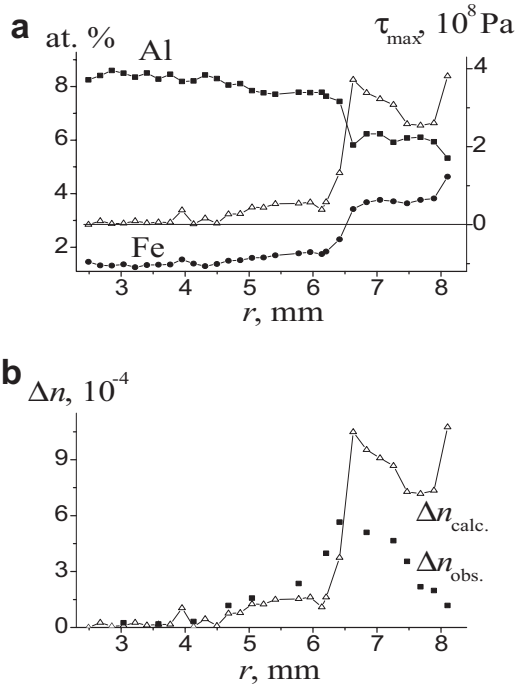

FIG. 5. Mismatch strain and anomalous birefringence in crystal #2. (*a*) Concentrations of Al and Fe and maximum shear stress τ_{max} as a function of crystal radius r. (*b*) Observed ($\Delta n_{obs.}$) and calculated ($\Delta n_{calc.}$) birefringence as a function of crystal radius r. The value of $\pi_{44} = 0.5\times10^{-12}$ Pa^{-1} is used.

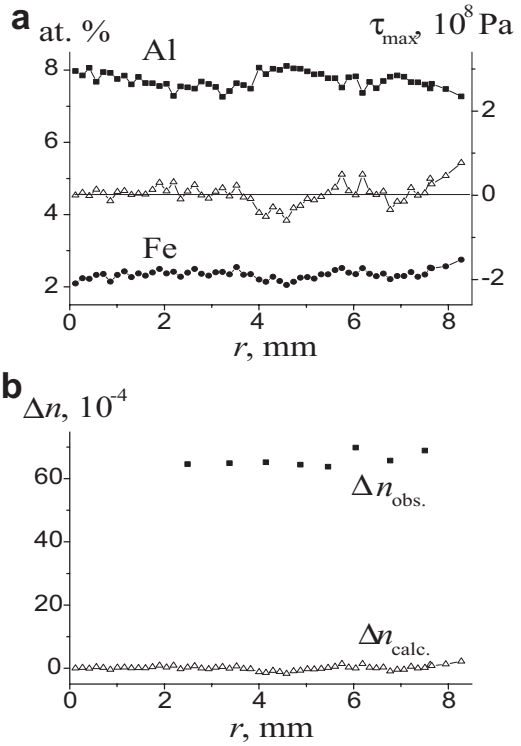

FIG. 6. Mismatch strain and anomalous birefringence in the crystal #3. (*a*) Concentrations of Al and Fe and maximum shear stress τ_{max} as a function of crystal radius *r*. (*b*) Observed ($\Delta n_{obs.}$) and calculated ($\Delta n_{calc.}$) birefringence as a function of crystal radius *r*. The value of $\pi_{44} = 0.5 \times 10^{-12}$ Pa^{-1} is used.

Crystal #2 (group 1) is characterized by smaller birefringence ($\Delta n_{obs} < 6 \times 10^{-4}$), which is in agreement with the calculated birefringence when the minimum, most likely value of piezo-optic coefficient ($\Delta n_{calc} = 5-10 \times 10^{-4}$) is used. The spatial distributions of calculated and observed birefringences in crystal #2 are also similar (Fig. 5). However, full coincidence is not achieved, especially near crystal edges. This discrepancy might be caused by brittle relaxation of elastic stress which manifests itself in numerous cracks and leads to the decrease of τ_{max} and Δn_{obs}.

An important peculiarity of crystal #2, and similar crystals from group 1, is the alternation of zones with indices of refraction a' and c' normal to the growth front. This confirms the mismatch strain origin of optical anomalies, since stress must change its sign at the zone boundary. Variations of extinction position and birefringence arise also near cracks. This proves the assertion that mismatch strain is the main cause of optical anomalies for this group of garnet crystals.

The birefringence for crystal #3 (group 2) is >10 times higher than for crystal #2 (Fig. 6). However, it is accompanied by much lower mismatch strain. Even with the extreme, unrealistic values of the piezo-optic coefficient, our calculation gives $\Delta n_{calc} = 1.4-27 \times 10^{-4}$. This value is significantly lower than the observed birefringence ($\Delta n_{obs} = 60-70 \times 10^{-4}$).

The anomalous birefringence in crystal #2 and other crystals of group 1 can be explained by mismatch strain only. The contribution of mismatch strain to crystal #3 and other crystals of group 2 is insufficient to explain their birefringence. There must, therefore, be another mechanism that generates birefringence in these garnets.

Growth dissymmetrization

General remarks

The second most likely cause of optical anomalies in grandite garnets is ordering of Al^{3+} and Fe^{3+} on *Y* sites. Ordering was found experimentally by X-ray structural analysis (Takéuchi *et al*., 1982; Kingma and Downs, 1989; Gali, 1983). However, the origin of this ordering remains to be established. It might be either a thermodynamic or a kinetic order-disorder phase transition. In the former case two phases with different fields of stability possess different states of order. A reversible transition between these two phases occurs under certain *P-T* conditions.

Kinetic phase transition, or so-called growth dissymmetrization, is realized as atom growth ordering. This hypothesis, proposed by Akizuki (1984), suggests that positions of atoms which are strictly equivalent in the volume of a crystal can be geometrically and energetically non-equivalent on the surface of a growing crystal. This can give rise to an ordered distribution of isomorphous atoms. The ordered state arising on the surface is then buried in the volume of a crystal in the course of its growth. This state is metastable but it can be retained in a crystal for a long time due to low diffusion rates. Thus, the symmetry of a crystal is lowered, and this can lead to optical anomalies.

Hatch and Griffen (1989) showed that the lowering of garnet symmetry could be explained by an order-disorder phase transition with a single

order parameter. However, these results do not contradict the hypothesis of kinetic phase transition. Data on the mixing energy could help to make a choice between these two types of transitions. Unfortunately, experimental results differ singnificantly from each other, suggesting slightly negative (Ganguly, 1976), positive (Engi and Wersin, 1987) or zero (Perchuk and Aranovich, 1979) enthalpy of mixing. Since a high negative value of the mixing enthalpy, intrinsic to thermodynamic order-disorder phase transition, was not revealed, we cannot adopt this hypothesis.

Although growth dissymmetrization is not known in detail, it is the most likely reason for anomalous birefringence in grandite garnets, there being much supporting experimental data (e.g. Akizuki, 1984; Allen and Buseck, 1988). Crystals with optical anomalies of this origin should be characterized by common features: i.e. distinctive orientation of the optical indicatrix; effects of crystal composition, growth temperature, growth rate and high temperature annealing; lowering of crystal symmetry (Shtukenberg and Punin, 1996), which, as we will demonstrate in the following paragraphs, are typical for grandite garnets.

Orientation of optical indicatrix

The orientation of the optical indicatrix depends on the structure and the orientation of growth front. Optical indicatrices of the different simple forms differ in their shape and orientation. Growth sectors of the same form possess similar indicatrices which differ in their orientation relative to a common crystallographic basis. Viewed between crossed polars, such crystals look like twins.

The orientation of the optical indicatrix for garnets with high birefringence (>0.001) remains approximately constant relative to the growth front orientation. Detailed study of the optical properties of crystal #3 shows that a is normal to the growth front (110), c is parallel to the axis [$\bar{1}$10] (long diagonal of (110) face) and b is parallel to the axis [001] (short diagonal of (110) face). The position of the axes is variable within a few (up to 15) degrees. The axial angle $2V\alpha$ is $(-)80^\circ$, and the birefringence measured in a thin-section cut parallel to the (001) face corresponds to maximal birefringence in the crystal $\Delta n = c - a$. The measured parameters of optical indicatrix are in a good agreement with those presented by Akizuki (1984) and Allen and Buseck (1988) for a few grandite garnets (angle between a and [110] varies in the range $0-11^\circ$; between c and [110]: $0-35^\circ$; between b and [001]: $0-35^\circ$; the axial angle $2V\alpha = 80-100^\circ$). Thus, the optical indicatrix has an approximately constant orientation and constant value of $2V\alpha$ for grandite garnets with high birefringence taken from various mines.

The orientation of the optical indicatrix depends also on the vicinal relief of a growing face. This results in subsector zoning. The observed wedge-like subzones visible in sections parallel to the growth direction (see above) can be considered as subsectors which are formed by different vicinal faces. Akizuki (1984) observed another type of optical subsector zoning in grandite garnets in sections parallel to growth faces {110}. In this case the crystal surface is divided into regions of rhomboid shape with different extinction directions which correspond to different slopes of growth hillocks. Good agreement between observed optical subsector zoning and vicinal relief was found by Akizuki (1984) for a number of crystals. These optical data are in a good agreement with the hypothesis of kinetic ordering of Al and Fe.

Effect of crystal composition and growth conditions

For the case of two cations ordering on two non-equivalent positions (here Al and Fe on two non-equivalent octahedral positions) the effect of crystal composition was considered theoretically (Shtukenberg *et al.*, 2000). The approach considers the distribution coefficients between these non-equivalent positions and growth solution and leads to the following parabolic relation $\Delta n \approx Kx(1-x)$, where K is a constant depending on the growth conditions. Our data, together with results from the literature (Fig. 7), do not follow the simple parabolic relationship between composition and birefringence predicted by theory. Instead, the data occupy a region of $\Delta n - x$ space that lies beneath the parabola (dashed line in Fig. 7). Reduction of the birefringence can be explained by the action of additional factors (such as growth temperature and growth and post-growth annealing) on the value of K, and as a result the maximum value of the birefringence for a given Fe/(Al + Fe) ratio is attained in only some crystals.

The rise of growth temperature and the annealing of a crystal may lead to the decay of optical anomalies or even to their disappearance, e.g. anomalous birefringence in alum mixed

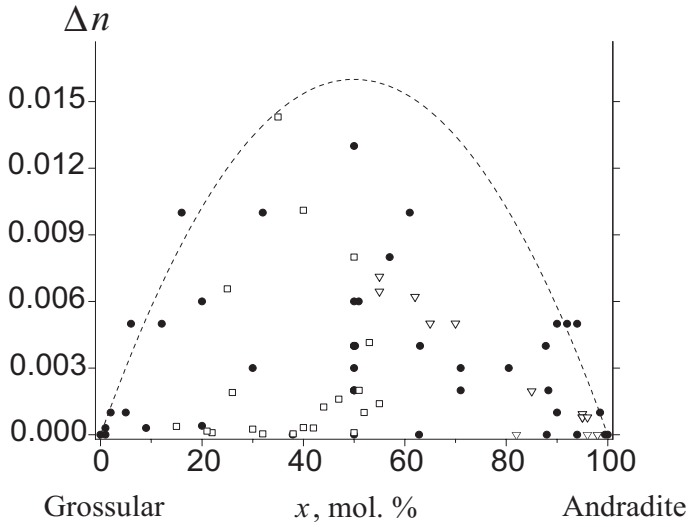

FIG. 7. The value of birefringence (Δn) as a function of composition (x) for grossular–andradite garnets. Open symbols represent our data and solid symbols literature data (Fraga *et al*., 1982; Kalinin, 1967; Takéuchi, 1982; Murad, 1976; Hirai and Nakazawa, 1982; Allen and Buseck, 1988; Griffen, 1992; Kingma and Downs, 1989; McAloon and Hofmeister, 1995; Hariya and Kimura, 1978). Theoretical dependence is shown by the dashed line.

crystals (Shtukenberg *et al*., 1998). We did not study these relations in grandite garnets experimentally. However, Hariya and Kimura (1978) noted the disappearance of birefringence upon high-temperature (600−900°C) annealing. Moreover, they showed that crystals synthesized at temperatures >700°C were isotropic, whereas crystals of the same composition grown at low temperatures were anisotropic.

Lowering of a crystal symmetry

Growth dissymmetrization leads to small structural distortions that are hard to detect using ordinary methods of X-ray crystallography. To prove the lowering of crystal symmetry it is necessary to investigate a number of indicators: deformation of the unit cell, differences in intensities of reflection that are equivalent in the Laue class $m\bar{3}m$, the presence of reflections that are forbidden in the space group $Ia\bar{3}d$. These indicators have been found in grandite garnets (Akizuki *et al*., 1998; Allen and Buseck, 1988; Badar and Akizuki, 1997; Hirai and Nakazawa, 1986; Takéuchi *et al*., 1982), but not all indicators were revealed in the same crystal.

In the present paper the lowering of the crystal symmetry was studied by the single crystal XRD method in three samples, two of which were cut from the rim and core, respectively, of crystal #1 (group 1, low birefringence) and the third from crystal #3 (group 2, high birefringence) – see Table 4.

The average lattice constants of the crystals studied (Table 4), $a_{aver.}$, coincide with those measured by the powder XRD method $a_{powd.}$ (Tables 3, 4). The differences beween values of a, b and c parameters do not exceed 0.003 Å, which is comparable with experimental errors of their determination (0.002−0.003 Å). The distortion of the cubic unit cell manifests itself as deviation of one of the axial angles (β) from 90°. The quantity β−90 reaches its maximum value, 0.12°, in crystal #3. This result corresponds with the data obtained by Takéuchi *et al*. (1982), Badar and Akizuki (1997) and Akizuki *et al*. (1998) on five birefringent grandite garnets. According to these data the value of β−90 varies in the range 0.07−0.14°. Other authors either found no distortion of the cubic unit cell (Griffen *et al*., 1992; Kingma and Downs, 1989) or revealed the difference (up to 0.012 Å) between linear lattice constants (Allen and Buseck, 1988).

The intensity differences of symmetrically equivalent reflections were analysed for 48 reflections which are symmetrically equivalent

TABLE 4. Birefringence, composition and lattice constants of the studied crystals.

Sample	Group	Birefringence ($\times 10^{-4}$)	Fe/(Fe+Al) (%)	Lattice constants								
				a (Å)	b (Å)	c (Å)	$a_{aver.}$ (Å)	$a_{powd.}$ (Å)	α°	β°	γ°	(β−90)°
1 (rim)	1	0.5	37	11.905(3)	11.903(3)	11.903(3)	11.904	–	89.99(2)	90.00(2)	90.00(2)	0.00(2)
1 (core)	1	2	26	11.914(3)	11.917(2)	11.914(2)	11.915	11.915(2)	90.00(2)	90.05(2)	90.00(2)	0.05(2)
3	2	60	23	11.892(2)	11.889(2)	11.892(2)	11.891	11.889(2)	90.00(2)	90.12(2)	90.03(2)	0.12(2)

Cell dimensions a, b, c, α, β and γ were determined with a four-circle autodiffractometer ($a_{aver.} = (a + b + c)/3$)
$a_{powd.}$ – with X-ray powder diffraction method

to reflection 615 in the cubic Laue class $m\bar{3}m$. Experimental intensity errors were estimated in two ways: (1) as standard deviations of intensities (σ_ψ) obtained by rotation (in 10° steps) of the crystal along the normal to the reflecting plane (ψ scanning); and (2) as a difference between inversionally symmetrical reflections $R_{\bar{1}} = I_{hkl} - I_{\bar{h}\bar{k}\bar{l}}$. It should be noted that an approximate relation $2\sigma_\psi \approx R_{\bar{1}}$ is fulfilled. This means that the effect of multiple diffraction, which is strong in garnets (Rossmanith and Armbruster, 1995), does not contribute significantly to the measured intensities. To find any violations of symmetry operations we grouped reflections which are equivalent relative to symmetry operations in the cubic Laue class $m\bar{3}m$, each group consisting of 2, 3 or 4 reflections for miror planes, three- and fourfold axes, respectively. The differences between minimal and maximal intensities within each group (I_{min} and I_{max}, respectively) have been compared with experimental errors σ_ψ. Figure 8 shows the fractions of these groups (P) for which $I_{max} - I_{min} > \sigma_\psi$. Symmetry operation violations are present in all three crystals. However, crystal #3 reveals the most violations of all symmetry operations, demonstrating the triclinic symmetry. The differences of equivalent intensities were found in other papers as well (Allen and Buseck, 1988; Hirai and Nakazawa, 1986; Takéuchi *et al*., 1982). The most detailed analysis was carried out by Takéuchi *et al*. (1982) who found violations of all symmetry operations in the Munam garnets, suggesting triclinic symmetry. However, in their experiment, violations of one coordinate plane and two diagonal ones were significanly weaker than of other planes. This highlights the closeness to orthorhombic Laue class *mmm*.

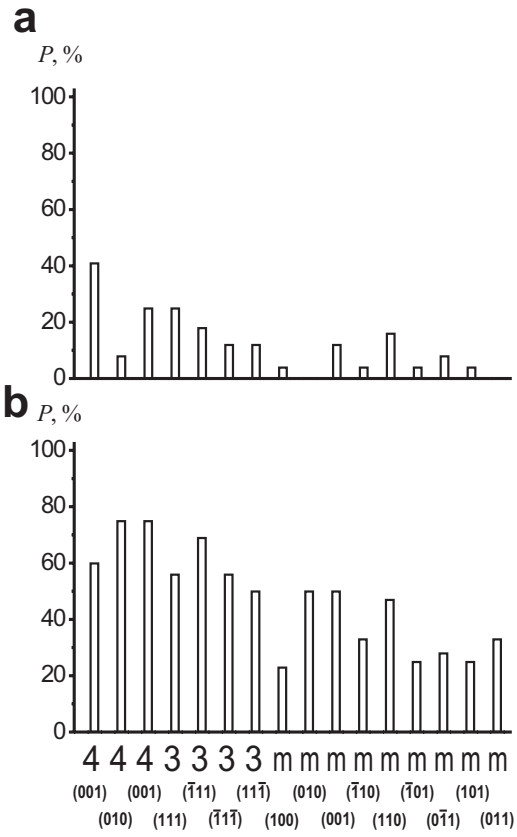

FIG. 8. Fraction of groups symmetrically equivalent in the cubic Laue class $m\bar{3}m$ reflections (P) for which $I_{max} - I_{min} > \sigma_\psi$ for the case of 615 reflections (the set of 48 reflections). Symmetry operations are written below the columns. (*a*) sample #1 (rim) and; (*b*) sample #3.

In order to check the presence of forbidden reflections, a set of ~50 (h00), (0k0) and (00l) reflections was collected. The presence of reflections forbidden in the Laue class $m\bar{3}m$ has been demonstrated by means of ψ scanning (Table 5). These reflections do not allow us to determine which symmetry operations have been violated, though none of these reflections contradict the body-centred lattice. The appearance of forbidden reflections in grandite garnets was revealed by Hirai and Nakazawa (1986) in samples from the Mull Kum mine. According to their data one *a* and two *d* glide planes remain in a crystal resulting in orthorhombic space group *Fddd*.

Thus, the results obtained demonstrate that the symmetry of all crystals studied is less than cubic, and the symmetry of crystal #3 is triclinic. The spatial distribution of abnormal birefringence in

TABLE 5. List of forbidden reflections in the samples studied. These reflections were revealed on the basis of measurements of coordinate reflections h00, 0k0 and 00l.

Sample	Observed forbidden reflections with $I_{obs.} > 4\sigma_I$
1 (rim)	006, 10 0 0
1 (core)	200, 020, 002
3	600, 060, 002, 020, 200

crystals (see above) suggests that symmetry lowering is the consequence of growth dissymmetrization. The partial ordering of Al and Fe in octahedrons is probably responsible for growth dissymmetrization, since the compositional variations in the crystals studied occurred only on *Y* sites (Table 1). This assertion was confirmed by Takéuchi *et al*. (1982), Kingma and Downs (1989) and Gali (1983), who detected the ordering of Al and Fe^{3+} in grandite garnets with optical anomalies.

Based on these results we conclude that the main cause of optical anomalies in garnet crystals with high birefringence (group 2) is probably growth dissymmetrization. The refinement of the crystal structure of crystal #3 (results to be published) confirms the triclinic symmetry of this crystal, reveals Al/Fe partial ordering on octahedral sites and, thus, supports our suggestion.

Conclusion

The complex anomalous optics of grandite garnets cannot be explained by a single mechanism. This phenomenon is the result of at least two fundamentally different mechanisms. They are: (1) growth dissymmetrization (probably caused by partial ordering of Al^{3+} and Fe^{3+} on *Y* sites, mechanism 1a); and (2) mismatch strain (mechanism 2). The appearance of optical anomalies due to the former was found by a few authors, e.g. Allen and Buseck (1988), whereas anomalies due to the latter have been proved by the present authors for the first time. Using abnormal optical properties only, we can identify the mechanism causing birefringence.

If the birefringence is of a relatively low magnitude (<0.001), the distribution of birefringence within a crystal is very complex and depends on the compositional inhomogeneity. If the crystal has a high dislocation density and numerous cracks, then anomalous birefringence is likely to be caused by mismatch strain. This corresponds to high growth temperature and to compositions near to the ends of the isomorphous series.

On the other hand, if birefringence is relatively high (up to 0.015) and the optical pattern and distribution of composition within a crystal are relatively simple, the main reason for optical anomalies is the growth ordering of cations (growth dissymmetrization). These peculiarities correspond to low growth temperature and to intermediate compositions.

In most cases, however, both mechanisms act simultaneously. The contribution of each mechanism to the overall optical pattern manifests itself in the mode of orientation of the vibration directions. If the value of birefringence is small ($\Delta n_{obs} = 0-2\times10^{-4}$) we can see, as a rule, the alternation of zones with c' or a' normal to the growth front, and this argues in favour of a predominance of stress birefringence. For the higher value of birefringence ($\Delta n_{obs} = 2-10\times10^{-4}$) these changes of a' orientation take place only in a few zones per crystal and a' is normal to the growth front in most zones. The contribution of each mechanism is approximately equal. For the crystals with maximum values of birefringence, a' is always normal to the growth front and growth dissymmetrization dominates over mismatch strain.

Acknowledgements

This work was supported by the Russian Fund for Basic Researches (projects #98-05-64151 and #00-05-65182) and by the programme 'Universities of Russia'. The authors wish to thank E. Nikandrova and Yu. Skalkina for help with the optical studies; Dr J. Zang for kindly providing samples; Yu.L. Krezer and L.S. Smolskaya for performing the electron microprobe analysis; Dr M.L. Zorina for performing the IR spectroscopy measurements; Dr A.E. Voloshin for the XRD topography studies; and Dr I.V. Rozhdestvenskaya and I.I. Bannova for performing the X-ray single crystal diffraction measurements.

References

Akizuki, M. (1984) Origin of optical variation in grossular-andradite garnet. *Amer. Mineral*., **69**, 328–38.

Akizuki, M., Takéuchi, Y., Terada, T. and Kudoh, Y. (1998) Sectoral texture of cubo-dodecahedral garnet in grandite. *Neues Jahrb. Mineral. Mh*., 565–76.

Allen, F.M. and Buseck, P.R. (1988) XRD, FTIR and TEM studies of optically anisotropic grossular garnets. *Amer. Mineral*., **73,** 568–84.

Badar, M.A. and Akizuki, M. (1997) Iridiscent andradite garnet from the Sierra Madre Mountains, Sonora, Mexico. *Neues Jahrb. Mineral. Mh*., 529–39.

Bird, D.K. and Helgeson, H.C. (1980) Chemical interactions of aqueous solutions with epidote-feldspar mineral assemblages in geologic systems. I. Thermodynamic analysis of phase relations in the

system CaO–FeO–Fe_2O_3–Al_2O_3–SiO_2–H_2O–CO_2. *Amer. J. Sci*., **280**, 907–41.

Blanc, Y. and Maisonneuve, J. (1973) Sur la biréffringence des grenats calciques. *Bull. Soc. Franc. Mineral. Cristallogr*., **96**, 320–21.

Brauns, R. (1891) *Die optischen Anomalien der Kristalle*. Preisschr. Jablonowski Ges., Leipzig, Germany.

Engi, M. and Wersin, P. (1987) Derivation and application of a solution model for calcic garnet. *Schweiz. Mineral. Petrogr. Mitt.*, **67**, 53–73.

Fraga, H., Gali, S. and Font-Altaba, M. (1982) Sector zoning as a growth phenomenon and its influence in the optical properties of crystals. The case of grossular-andradite garnets. *Estudios Geol.*, **38**, 173–78.

Gali, S. (1983) Grandite garnet structures in connection with the growth mechanism. *Z. Kristallogr*., **163**, 43–52.

Ganguly, J. (1976) The energetics of natural garnet solid solutions: II. Mixing of the calcium silicate end-members. *Contrib. Mineral. Petrol*., **55**, 81–90.

Gorskaya, M.G., Punin, Yu.O., Sokolov, P.B. and Kretser, Yu.L. (1992) Inhomogeneity of composition and heterometry in crystals of polychromic tourmalines. *Mineral. J*., **14**, 3–10 (in Russian).

Griffen, D.T., Hatch, D.M., Phillips, W.R. and Kulaksiz, S. (1992) Crystal chemistry and symmetry of birefrigent tetragonal $pyralspite_{57}$–$grandite_{25}$ garnets. *Amer. Mineral*., **77**, 399–406.

Hatch, D.M. and Griffen, D.T. (1989) Phase transition in the grandite garnets. *Amer. Mineral*., **74**, 151–59.

Hariya, Y. and Kimura, M. (1978) Optical anomaly garnet and its stability field at high pressure and temperatures. *J. Fac. Sci., Hokkaido University, series IV*., **18**, 611–24.

Hirai, H. and Nakazawa, H. (1982) Origin of iridescence in garnet: An optical interference study. *Phys. Chem. Miner*., **8**, 25–28.

Hirai, H. and Nakazawa, H. (1986) Visualising low symmetry of a grandite garnet on precession photographs. *Amer. Mineral.*, **71**, 1210–3.

Kalinin, D.V. (1967) On the relations between anisotropic garnets with the composition and chemical environment during their synthesis. *Dokl. Akad. Sci*., **172**, 1167–70 (in Russian).

Kingma, K.J. and Downs, J.W. (1989) Crystal-structure of a birefringent andradite. *Amer. Mineral*., **74**, 1307–16.

Landolt, H. and Börnstein, R. (1979) *Numerical Data and Functional Relationships in Science and Technology. Elastic, Piezoelectric, Pyroelectric, Piesooptic, Electrooptic Constants and Nonlinear Dielectric Susceptibilities of Crystals. New Series, Group III*, **11**, Springer, Berlin, Heidelberg, New York.

Lessing, P. and Standish, R.P. (1973) Zoned garnet from Crested Butte, Colorado. *Amer. Mineral*., **58**, 840–2.

McAloon, B.P. and Hofmeister, A.M. (1995) Single-crystal IR spectroscopy of grossular-andradite garnets. *Amer. Mineral*., **80**, 1145–56.

Murad, E. (1976) Zoned, birefringent garnets from Thera Island, Santorini Group (Aegean Sea). *Mineral. Mag*., **40**, 715–9.

Novak, G.A. and Gibbs, G.V. (1971) The crystal chemistry of the silicate garnets. *Amer. Mineral*., **56**, 791–825.

Nye, J.F. (1957) *Physical Properties of Crystals*. Clarendon Press, Oxford, UK.

Perchuk, L.L. and Aranovich, L.Y. (1979) Thermodynamics of minerals of variable composition: Andradite-grossularite and pistacite-clinozoisite solid solutions. *Phys. Chem. Miner*., **13**, 1–14.

Rossman, G.R. and Aines, R.D. (1986) Birefrigent garnet from Asbestos, Quebec, Canada. *Amer. Mineral*., **71**, 779–80.

Rossmanith, E. and Armbruster, T. (1995) The intensity of forbidden reflections of pyrope: Umweganregung or symmetry reduction? *Zeits. Kristallogr*., **210**, 645–9.

Shannon, R.D. (1976) Revised effective ionic radii and systematic studies of interatomic distances in halides and chalcogenides. *Acta Crystallogr*., **A32**, 751–67.

Shtukenberg, A.G. and Punin, Yu.O. (1996) Optical anomalies in crystals. *Zap. Vseross. Miner. Obshch*., **125**, 104–20 (in Russian).

Shtukenberg, A.G., Punin, Yu.O. and Kovalev, O.G. (1998) Temperature behavior of optical anomalies in alum crystals. *Cryst. Rep*., **43**, 465–8.

Shtukenberg, A.G., Punin, Yu.O. and Soloviev, V.N. (2000) Effect of growth conditions on the birefringence of mixed crystals revealed in alum solid solutions. *Mineral. Mag*., **64**, 837–45.

Takéuchi, Y., Haga, N., Umizu, S. and Sato, G. (1982) The derivative structure of silicate garnets in grandite. *Zeits. Kristallogr*., **158**, 53–99.

Vorobiev, Yu.P. (1989) Structural, magnetic and thermophysical properties of garnets. *Cryst. Rep*., **34**, 1461–9.

[*Manuscript received 18 September 2000: revised 16 March 2001*]